Chapter 7

Stress Analysis of Electrode Particles in Lithium-Ion Batteries

Yingjie Liu and Huiling Duan

Additional information is available at the end of the chapter

http://dx.doi.org/10.5772/62577

Abstract

This chapter reviews several theoretical models that are used to compute the stress fields inside the electrode particles of lithium-ion batteries during discharging/charging process and provides a guideline for researchers to choose the appropriate models. Due to the limitation of the existing models, a general electrochemo-mechanical framework is presented to model the concentration and stress fields of the electrode during the phase transformation. The interaction between stresses fields and phase transformation is addressed, which is a novel discovery in the research of lithium-ion batteries. The electrodes with different sizes and geometries are compared. The structural and electrochemical advantages of hollow core-shell structure particles are highlighted. The present work could help to accurate predict stress profile in electrode particles with different sizes, geometries, and charging operations and contributes to finding the optimal electrode. Therefore, this chapter is helpful for the material and structure design of electrodes of lithium-ion batteries.

Keywords: lithium-ion batteries, surface/interface stress, hydrostatic stress, phase transformation, core-shell electrode

1. Introduction

Lithium-ion batteries are the choices of diverse applications, such as electronics and electric cars because of their high capacity, high voltage, and long lifetime, and attract wide research interest in the community of chemistry, electro-chemistry, and mechanics [1–6]. During the process of charging/discharging, lithium ions insert into/extract from electrodes and induce high stresses [7]. The stress could cause the fracture of electrode when it exceeds the ultimate strength of

the material [8–10]. This intercalation-induced fracture is indeed a key mechanism for lithium-ion battery's capacity fade.

To prevent this stress-induced electrode failure, accurate prediction of the stress fields is the first step. Therefore, multiple models are developed to address the effects of different factors on the stress field, e.g., hydrostatic stress [7], surface stress [11], charging operation [12, 13], material imperfection [14], plasticity [15, 16], heat generation [17, 18], particles' dissolution [19, 20]. Inserting the stress field into the fracture mechanics model, some novel models are proposed to investigate the electrode fracture and battery failure. For instance, Woodford et al. [14] calculates the stress intensity factor of the initial crack inside the electrode and the stability of crack growth. Several novel models are developed to predict the dynamic crack propagation [21–23]. The effects of some factors cannot be characterized by continuum models, which motivates some atomic scale research. Gao et al. developed the atomistic models to study the strong coupling of diffusion, stress, and solute concentration, and the surface locking instability during atomic intercalation into electrode [24, 25]. Suo et al. employed the first principle calculation to investigate the microscopic deformation and lithiation induced plasticity of silicon electrode [26, 27].

Phase transformation during the discharging/charging process has been widely reported in different electrode active materials [28, 29]. During the phase transformation, the electrode is divided into two phases by a phase interface. Because the equilibrium concentration of the two phases at the interface is different, an interface concentration discontinuity is observed. This phase interface is moving during the phase transformation, whose movement is characterized by an interface mass balance condition. Though this phase transformation can be tracked by the moving boundary models [30–33], the stress fields during the phase transformation are not well studied. Moreover, the effect of stress fields on phase transformation remains unknown. This chapter will systematically investigate the interactions between phase transformation and stress fields.

The second step to avoid the stress-induced electrode failure is to find an optimal electrode to lower the stress. The main research interests focus on the size and shape of the electrodes. Considerable efforts are put into studying the size of electrodes [25, 34]. The major conclusions are that nanoelectrode particles are not as easy to fail as micro ones, and the batteries with nanoelectrode particles have better cyclability. However, researchers obtain this conclusion by using the same models to analyze the behaviors of different-sized particles, which is incorrect. For example, the linear diffusion model [17] is only accurate for nanoelectrode particles while loses accuracy for large electrode particles. A comprehensive model that could provide accurate stress prediction for different sized electrode particles is needed. In terms of electrode shape, though researchers have tested the electrode particles of different shapes, e.g., spherical [34], core-shell [35, 36], nanowire [37], thin film [38, 39], layered plates [40], thin strip [41], and cylinder [42], it is still an open question what an optimal electrode is.

Hollow structure particle is a good candidate for the electrode of lithium-ion batteries, due to its unique structural properties, e.g., doubled surface area, core-shell structure, and large internal void [43]. Researchers have analyzed the mechanical properties of core-shell structure [44, 45], and emphasized its significant influence on the stress fields. Furthermore, the

advantages of hollow structure particles are highlighted by numerous experiments, when they are used as electrode particles. For example, hollow Si anode shows high initial discharging capacity and low-capacity degradation [46]. High capacity, good cyclability, and high rate capability are reported for hollow core-shell mesoporous TiO_2 spheres [48]. High coulombic efficiency, great rate performance, and excellent stability are observed in hollow Fe_2O_3 particles [49]. However, these works reveal few reasons for the optimal behaviors of hollow structure particles. Therefore, a comprehensive analysis is needed to investigate the properties of hollow structure electrode. In this chapter, a theoretical model on the hollow particles is introduced which considers the effects of hydrostatic stress, surface/interface stress, and phase transformation simultaneously.

In what follows, Section 2 briefly reviews the recently developed models on the stress fields of electrode particles. A guideline is proposed for researchers to choose appropriate models. Section 3 presents an electrochemo-mechanical framework to model the concentration and stress profile in the electrode of Lithium-ion batteries. The effects of hydrostatic stress, surface/interface stress, and phase transformation are fully coupled. Section 4 applies this framework to the hollow spherical electrode particle and calculates its concentrations and stress fields. In Section 5, the size and shape effects of electrode are analyzed to find the optimal electrode. Size effects induced by hydrostatic stress and surface/interface stresses are investigated through a cross-scale analysis, and shape effect is studied by varying the shell thickness. The structural and electrochemical advantages of hollow structure electrodes are investigated. Finally, some remarkable conclusions and discussions are provided in Section 6.

2. Review of existing models

To provide accurate predictions of the stress fields in the electrodes, multiple models are developed to address the effects of different factors on the stress field. This section briefly introduces some recently developed models and provides a guideline for researchers to choose appropriate models.

Zhang et al. [18] considers the effect of hydrostatic stress on the lithium flux, which provides accurate predictions on the stress fields. However, this effect is only important for micro electrode particles and can be ignored for nano ones. When the particle size is in nanoscale, Cheng et al. [11] reports the effect of surface stress, which is inversely proportional to the particle size. This surface effect is essential for nanoelectrode particles because it changes the stress state from traction free into compression and therefore prevents the growth of manufacture induced cracks. Therefore, the model with hydrostatic stress suits the research on micro electrode particles while the surface stress is a good choice for nano ones. Cheng et al. [12] and Lu et al. [50] investigate the influence of charging operations on stress fields, i.e., potentiostatic and galvanostatic operation. The galvanostatic process is the first stage of the charging process and occupies over 90% of the entire charging time and is commonly used in different models. However, there is some unused lithium ions at the end of galvanostatic process. To avoid the waste of the unused lithium, potentiostatic operation is needed. Therefore, potentiostatic operation is appropriate for the research on improving the battery efficiency.

The strain approximation is slightly different in modeling the cathode and anode. When modeling the cathode, since the deformation is small, the infinitesimal strain assumption is well accepted [14, 18, 35, 36]. However, during the charging/discharging process, the deformation of anode is large, especially when the anode material is silicon. Therefore, finite strain approximation is more reasonable in modeling the deformation of anode. The constitutive law is most important for the stress modeling, since it directly relates the stress state and deformation. Linear elastic assumption is usually the choice, since it is the simplest and the deformation of electrode particles usually stays in the elastic range. However, when the deformation is large enough, the stress can exceed the yielding criterion and the deformation may reach plastic scope. Therefore, linear elastic models are used for small deformation modeling, while plastic models are usually employed in modeling large deformation of electrode [15, 16].

Manufacture-induced initial flaws or cracks are important reasons for the failure of electrodes and therefore need to be carefully addressed. Stress concentration appears at these imperfections, and the growth of the imperfections could lead to the fracture of the electrodes. Woodford et al. proposes a fracture mechanics model to predict the stress fields at the initial crack [14]. However, this model can only determine whether the initial crack would grow. To model the dynamic crack propagation progress, multiple fracture models are developed [21–23]. In addition to cracks, one can investigate other failure mechanisms of the electrodes, e.g., delamination [13, 50], by inserting the stress fields into the corresponding models.

Phase transformation is experimentally observed in the electrode active material during discharging/charging process and could significantly affect the stress fields [30–32]. Multiple models have been developed to address the phase transformation-induced discontinuities in concentration and stress fields. However, the inverse effect of the stress fields on the phase transformation has not been well studied, until the recent work of current authors [47]. Liu et al. [47] proposes a fully coupled system which investigates the interactions between phase transformation and stress fields, which will be discussed in this chapter.

In the following, this chapter proposes an electrochemo-mechanical framework to model the concentration and stress fields of electrode particles. The interactions between stress fields and phase transformations are characterized. The effect of hydrostatic stress, surface stress, and interface stress are fully addressed.

3. Electrochemo-mechanical framework

There are three different stages in the whole discharging process, which are schematically illustrated in **Figure 1**. In the first stage, there is α phase only (c.f. **Figure 1a**). The lithium ion inserts into the electrode particles from the outer surface, and its concentration increases with time. This stage finishes when the concentration at the outer surface reaches the equilibrium value of α phase (c_{eq}^{α}). In the second stage, the α phase electrode material gradually transforms into β phase material, and the two phases are separated by a sharp phase interface $S_{\alpha\beta}$ (c.f. **Figure 1b**). The concentrations of the two phases equal their equilibrium values at the interface,

http://dx.doi.org/10.5772/62577

i.e., $c^{\alpha}\big|_{S_{\alpha\beta}}=c^{\alpha}_{eq}$, and $c^{\beta}\big|_{S_{\alpha\beta}}=c^{\beta}_{eq}$. Because $c^{\alpha}_{eq}\neq c^{\beta}_{eq}$, a concentration discontinuity appears at the interface. The flux is also discontinuous at the phase interface, which drives the interface to move inward. The phase transformation finishes when the material of the whole electrode particle changes into β phase. At this time, the concentration of lithium ions at the inner surface equals c^{β}_{eq}. The third stage is similar to the first one, in which there is β phase only in the electrode particle and the concentration increases with time (c.f. **Figure 1c**). Please note that the charging process can also be divided into three stages: (1) β phase only, (2) biphase, (3) α phase only, and therefore is the opposite process of discharging.

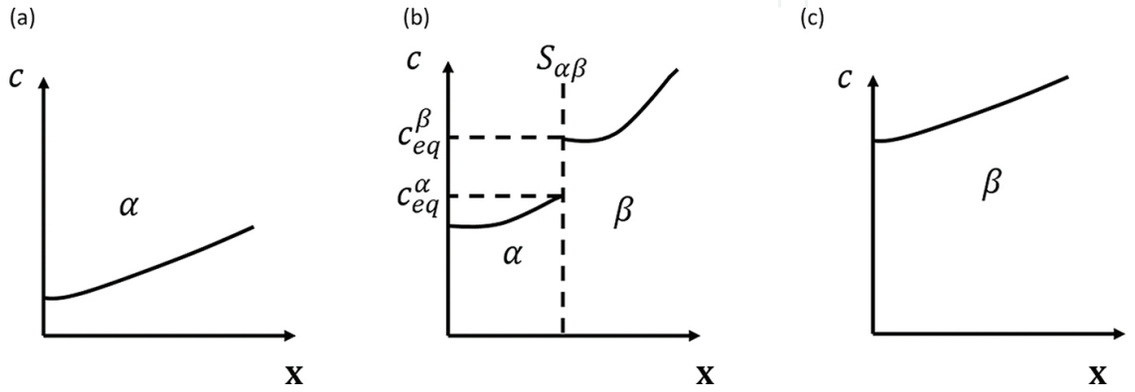

Figure 1. Schematic illustration of lithium concentration inside the electrode particle during discharging process: (a) first stage, there is α phase only and the concentration is continuous; (b) second stage, α and β phases coexist and are separated by a sharp interface $S_{\alpha\beta}$ at which the concentration is discontinuous; (c) third stage, there is β phase only. Please note that the concentration is discontinuous at second stage. Here x and c denote the position and lithium ions' concentration, c^{α}_{eq} and c^{β}_{eq} represent the equilibrium values of the two phases.

3.1. Mechanical equations

As illustrated in Figure **1**b, a phase interface $\mathbf{S_{\alpha\beta}}$ appears in the second stage of the discharging process. The electrode particle is separated into $\boldsymbol{\alpha}$ and $\boldsymbol{\beta}$ phases by $\mathbf{S_{\alpha\beta}}$ (c.f. **Figure 2**). Inserting lithium ions' into and extracting them from the electrode particle will cause its non-uniform distribution and then induce stress fields. Therefore, the concentration of lithium ions is considered in the constitutive law to characterize this mechanics-electrochemical coupling problem. For both $\boldsymbol{\alpha}$ and $\boldsymbol{\beta}$ phases, the constitutive law can be written as [50]

$$\boldsymbol{\varepsilon}^{p}=\frac{1}{E^{p}}\left[\left(1+\nu^{p}\right)\boldsymbol{\sigma}^{p}-\nu^{p}\Theta^{p}\boldsymbol{I}\right]+\frac{\tilde{c}^{p}\Omega^{p}}{3}\boldsymbol{I},\quad\left(p=\alpha,\beta\right) \tag{1}$$

where $\boldsymbol{\varepsilon}^{p}$ and $\boldsymbol{\sigma}^{p}$ denote strain and stress tensors of phase p, and $\Theta^{p}=\sum_{k}\sigma^{p}_{kk}$. E^{p}, ν^{p} and Ω^{p} are the Young's modulus, Poisson's ratio, and partial Molar volume of phase p, respectively. is the change of lithium ion's concentration $c^{p}(x, t)$ from the initial value $c^{p}_{0}(x)$ in the electrode

particles. Here, and in the following, the superscript p = α, β denote the α and β phases, respectively.

Classical elasticity theory yields the equilibrium equation,

$$\nabla \cdot \boldsymbol{\sigma}^p = 0 \tag{2}$$

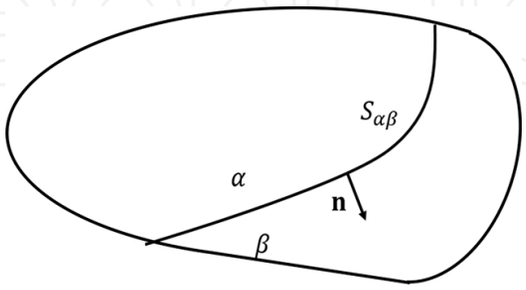

Figure 2. Schematic illustration of electrode particle: an interface $S_{\alpha\beta}$ separates the electrode particle into α and β phases.

and the infinitesimal strain geometric equation

$$\boldsymbol{\varepsilon}^p = \frac{1}{2}\left(\nabla \boldsymbol{u}^p + \boldsymbol{u}^p \nabla\right) \tag{3}$$

where $\mathbf{u^p}$ is the displacement vector of phase p.

Combination of Eqs. (1)–(3) yields the governing equation of each phase. In addition to the equations of two bulk phases, the deformation of interface needs to be characterized. The equilibrium equation of the phase interface $S_{\alpha\beta}$ is [51]

$$\left[\boldsymbol{\sigma}\right] \cdot \boldsymbol{n} = -\nabla_s \cdot \boldsymbol{\tau} \tag{4}$$

where $[\boldsymbol{\sigma}] = \boldsymbol{\sigma}^{\beta}\big|_{S_{\alpha\beta}} - \boldsymbol{\sigma}^{\alpha}\big|_{S_{\alpha\beta}}$, $\boldsymbol{\sigma}^{\alpha}$ and $\boldsymbol{\sigma}^{\beta}$ are the stress tensors of two phases, respectively. $\nabla_s \cdot \boldsymbol{\tau}$ denotes the interface divergence of interface stress $\boldsymbol{\tau}$ at the phase interface. Please note that stress discontinuity was only considered at the interface of two materials before [51–54], and the present chapter introduces the stress discontinuity at the phase interface of electrode in lithium-ion battery.

The interface constitutive law yields the relation between interface stress tensor $\boldsymbol{\tau}$ and interface strain tensor $\boldsymbol{\varepsilon^s}$

$$\boldsymbol{\tau} = \tau^0 1 + \boldsymbol{C}^s : \boldsymbol{\varepsilon}^s \tag{5}$$

http://dx.doi.org/10.5772/62577

where τ^0 is the strain-independent interface stress, **1** is a 2D second-order unit vector, and $\mathbf{C}^s$ is the interface stiffness tensor. Here and in the following, the super-subscript "s" denotes the interface/surface quantities.

The two phases are fully bonded at the interface, which yields the no jump condition

$$\boldsymbol{u}^{\alpha}\Big|_{S_{\alpha\beta}} = \boldsymbol{u}^{\beta}\Big|_{S_{\alpha\beta}} \tag{6}$$

where $\mathbf{u}^{\alpha}$ and $\mathbf{u}^{\beta}$ are the displacement vectors of two phases, respectively. Solving Eqs. (1)–(3) for α and β bulk phases, and Eqs. (4)–(6) for the interface $S_{\alpha\beta}$, one can compute the stress profile of the biphase electrode particle.

3.2. Electrochemical equations

Lithium ions extract from/insert into electrode particles during the charging/discharging process. This process is usually modeled as the diffusion of lithium ions, driven by the gradient of chemical potential. The velocity ($\mathbf{V}^p$) of lithium ions in phase p can be written as follows [18]:

$$\boldsymbol{V}^{p} = -M^{p}\nabla\phi^{p}, \quad \left(p = \alpha,\beta\right) \tag{7}$$

where $\mathbf{M}^p$ and ϕ^p are the mobility and electrochemical potential. The species flux ($\mathbf{J}^p$) is

$$\boldsymbol{J}^{p} = c^{p}\boldsymbol{V}^{p} = -c^{p}M^{p}\nabla\phi^{p} \tag{8}$$

where the electrochemical potential ϕ^p in an ideal solid solution is [18],

$$\phi = \phi_0^p + RTlnX - \Omega^p\sigma_h^p \tag{9}$$

where ϕ_0^p is a constant, R is gas constant, T is absolute temperature, X is molar fraction of lithium ion, and σ_h^p is hydrostatic stress,

$$\sigma_h^p = \frac{1}{3}\sigma_{kk}^p \tag{10}$$

Substituting Eq. (9) into Eq. (8), one obtains the species flux,

$$\boldsymbol{J}^{p} = -M^{p}c^{p}\left(RT\frac{1}{X}\nabla X - \Omega^{p}\nabla\sigma_h^p\right) = -D^{p}\left(\nabla c^{p} - \frac{\Omega^{p}c^{p}}{RT}\nabla\sigma_h^p\right) \tag{11}$$

where $D^p = M^pRT$ is diffusivity. Please note that the effect of hydrostatic stress on the species flux was neglected by previous work [11, 12, 41, 42], and is first proposed in [18]. The equation of substance conservation is written as

$$\frac{\partial c^p}{\partial t} + \nabla \cdot \boldsymbol{J}^p = 0 \tag{12}$$

Inserting Eq. (**11**) into Eq. (**12**), the governing equation of Li ions' concentration is obtained,

$$\frac{\partial c^p}{\partial t} - D^p \left(\nabla c^p - \frac{\Omega^p c^p}{RT} \nabla \sigma_h^p \right) = 0 \tag{13}$$

The boundary conditions are determined by the charging operation. Under galvanostatic operation,

$$\boldsymbol{J}^p \cdot \boldsymbol{n} = \frac{i_n}{F}(\text{active}); \quad \boldsymbol{J}^p \cdot \boldsymbol{n} = 0(\text{inactive}) \tag{14}$$

where $\mathbf{n}$ is the out normal of the boundaries. F is Faraday constant and $\mathbf{i_n}$ is currency density, respectively. When phase transformation begins, a phase interface appears between $\boldsymbol{\alpha}$ and $\boldsymbol{\beta}$ phases, as illustrated by Figure **2**. At the phase interface, the concentration of each phase equals its equilibrium value, i.e.,

$$c^\alpha \Big|_{S_{\alpha\beta}} = c_{eq}^\alpha; \quad c^\beta \Big|_{S_{\alpha\beta}} = c_{eq}^\beta \tag{15}$$

The movement of the phase interface is assumed to be under the control of diffusion process in the adjacent phases, and the interface position is tracked by a jump material balance [56],

$$\left(c_{eq}^\alpha - c_{eq}^\beta \right) \boldsymbol{v} \cdot \boldsymbol{n}^\alpha = \left(\boldsymbol{J}^\alpha - \boldsymbol{J}^\beta \right) \cdot \boldsymbol{n}^\alpha \tag{16}$$

where $\mathbf{v}$ is moving velocity of the phase interface, while $\mathbf{n}^\alpha$ is the normal direction from phase α pointing to phase β. Therefore, $\mathbf{v} \cdot \mathbf{n}^\alpha = \mathbf{v_n}$ is normal velocity which is negative in the discharging process and positive in the charging process. Noted that Eq. (16) is automatically satisfied when there is only one phase in the particle. Substitution of Eq. (11) into (16) yields the governing equation of the interface,

$$\left(c_{eq}^{\alpha}-c_{eq}^{\beta}\right)v_n = D^{\beta}\left(\frac{\partial c^{\beta}}{\partial n}-\frac{\Omega^{\beta}c^{\beta}}{RT}\frac{\partial \sigma_h^{\beta}}{\partial n}\right)-D^{\alpha}\left(\frac{\partial c^{\alpha}}{\partial n}-\frac{\Omega^{\alpha}c^{\alpha}}{RT}\frac{\partial \sigma_h^{\alpha}}{\partial n}\right) \tag{17}$$

where $\partial/\partial n$ denotes the gradient along the normal direction of interface. Please note that the effect of σ_h on the movement of phase interface has not been proposed in the literature [40, 41].

The electrode particle is initially at the stress free state, which implies that the initial concentration is uniformly distributed, i.e.,

$$c^{p}\left(t=0,x\right)=c_0 \tag{18}$$

A general electrochemo-mechanical framework is developed for an electrode particle of arbitrary geometry in lithium-ion batteries. The discharging/charging process can be regarded as a quasi-static process. In each time step, by inserting the concentration of Li ions into Eqs. (1)–(6), one can compute the stress field. Substituting the stress field into Eqs. (13)–(17), one can obtain the concentration field.

4. Stress field in hollow spherical electrode particle

Section 3 provides a electrochemo-mechanical framework to compute the concentration and stress profile for an electrode particle of arbitrary geometry in lithium ion batteries. This section will perform analysis on the concentration and stress fields of a specific electrode particle. Hollow structures have great potential as electrode of lithium-ion batteries, due to their better cyclability, higher capability, and lower capacity degradation [46, 48, 49]. Therefore, in the following, we will analyze the concentration and stress fields of the hollow electrode particles.

Figures 3 illustrate the structure of hollow spherical particles, r_1 and r_2 are the inner and outer radii of the hollow particles, respectively. $\zeta = r_1/r_2$ denotes the ratio of inner and outer radii. As emphasized in last section, α and β phases coexist in the electrode particle in the second stage of discharging process (c.f. **Figure 3a**). For this biphase particle, the inner layer is α phase and the outer one is β phase, which are separated by a sharp interface. Please note that the biphase electrode particle reduces to a single-phase electrode particle, when the phase interface overlaps with the outer/inner surfaces (c.f. **Figure 3b and 3c**). In what follows, the proposed electrochemo-mechanical framework in section 3 is applied on this specific hollow spherical particle electrodes, and the concentration and stress fields are analyzed.

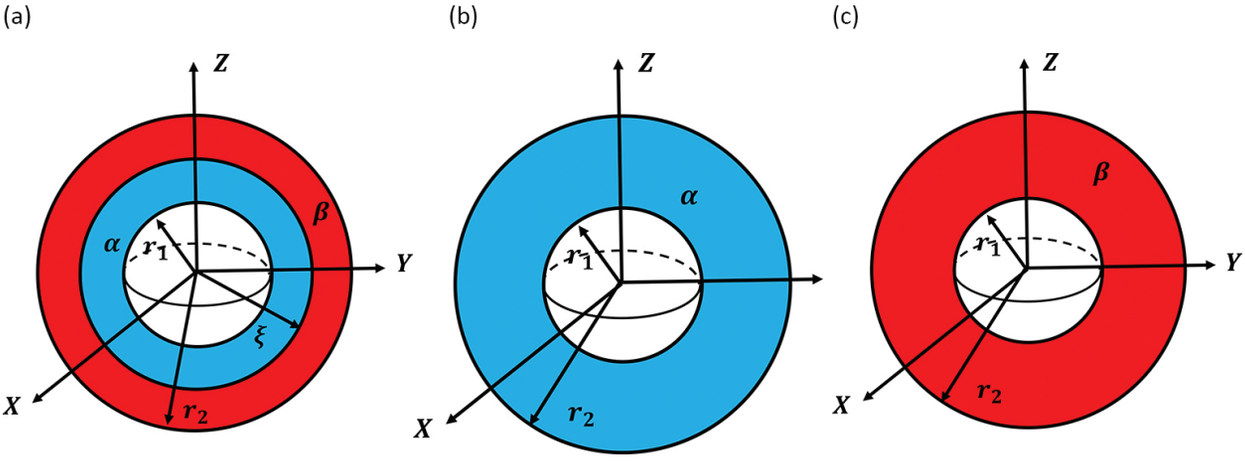

Figure 3. Three stages of the hollow $LiCoO_2$ particles in discharging process: (a) α and β phases coexist; (b) α phase only; (c) β phase only (reproduction from [47]).

4.1. Electrochemo-mechanical framework of hollow particle

As an axisymmetric problem, the displacement vector only has radial component (u) and the stress and strain tensors only contain two independent components σ_r , σ_θ and ε_r , ε_θ (note $\sigma_\phi = \sigma_\theta$, $\varepsilon_\phi = \varepsilon_\theta$). Under the spherical coordinate, Eqs. (1)–(3) become

Constitutive Law:

$$\begin{cases} \varepsilon_r^p = \dfrac{1}{E^p}\left(\sigma_r^p - 2\nu^p\sigma_\theta^p\right) + \dfrac{\Omega^p}{3}\tilde{c}^p \\ \varepsilon_\theta^p = \dfrac{1}{E^p}\left(\sigma_\theta^p - 2\nu^p\left(\sigma_r^p + \sigma_\theta^p\right)\right) + \dfrac{\Omega^p}{3}\tilde{c}^p \end{cases} \tag{19}$$

Equilibrium equation:

$$\frac{d\sigma_r^p}{dr} + \frac{2}{r}\left(\sigma_r^p - \sigma_\theta^p\right) = 0 \tag{20}$$

Geometric equation:

$$\varepsilon_r^p = \frac{du^p}{dr}; \quad \varepsilon_\theta^p = \frac{u^p}{r} \tag{21}$$

Combining Eq. (19)–(21), one could solve for the stress fields, i.e.,

$$\begin{cases} \sigma_r^p = E^p\left[\dfrac{-2}{1-\nu^p}\dfrac{\Omega^p}{9}c_{av}^p + \dfrac{A^p}{1-2\nu^p} - \dfrac{2B^p}{r^3\left(1+\nu^p\right)}\right] \\ \sigma_\theta^p = E^p\left[\dfrac{1}{1-\nu^p}\dfrac{\Omega^p}{9}c_{av}^p - \dfrac{1}{1-\nu^p}\dfrac{\Omega^p}{3}\tilde{c} + \dfrac{A^p}{1-2\nu^p} + \dfrac{B^p}{r^3\left(1+\nu^p\right)}\right] \end{cases} \tag{22}$$

where $c_{av}^p = \frac{3}{r^3}\int_{r_1^p}^{r} r^2 dr$. Please note that $r_1^\alpha = r_1$ and $r_1^\beta = \xi$, and ξ is the position of interface. A^p, B^p are constants that need to be determined via the boundary conditions.

When α and β phase coexist, there is a phase interface appearing at $r = \xi$. Figure 3a provides a schematic illustration of the phase distribution at this stage.

For the hollow spherical electrode particle, the interface equilibrium Eq. (4) is given as

$$\left(\sigma_r^\beta - \sigma_r^\alpha\right)|_{r=\xi} = \frac{2\tau_\theta}{\xi} \tag{23}$$

For the isotropic interface, the interface constitutive law Eq. (5) is

$$\tau_\theta = \tau^0 + K^s \varepsilon_\theta^p \tag{24}$$

where K^s is interface modulus ($\varepsilon_\phi^p = \varepsilon_\theta^p$). The displacement continuity Eq. (6) reduces to,

$$u^\alpha\Big|_{r=\xi} = u^\beta\Big|_{r=\xi} \tag{25}$$

The surface stress is effected via the boundary condition [55],

$$\sigma_r^p\Big|_{r=r_1} = \frac{2\tau_\theta}{r_1}; \quad \sigma_r^p\Big|_{r=r_2} = \frac{2\tau_\theta}{r_2} \tag{26}$$

It is noted that this boundary condition can be regarded as the special case of Eq. (4), when the interface is located at the inner and outer surfaces.

The constants A^α, B^α, A^β, and B^β are determined by solving Eqs. (23)–(26). Inserting them into Eq. (22), one can calculate the stress. When there is only α or β phase in the electrode particle, $A^\alpha = A^\beta$, $B^\alpha = B^\beta$, and Eq. (25) is automatically satisfied. In this case, phase interface ξ can be

regarded as r_2 for electrode with α phase only, while as r_1 for β phase only (illustrated by Figures 3b and 3c). Moreover, the interface condition Eq. (23) is automatically satisfied for the single phase electrode particle because it can reduce to the boundary condition Eq. (26). Therefore, one can obtain the solution of the single phase particle by setting ξ equals r_2 (α phase only) or r_1 (β phase only) in the solution of biphase particle.

The stresses inside the electrode particles are induced by the non-uniform distribution of concentration, which is studied by an electrochemical model. In the first and third stages of the discharging process, there is only α or β phase in the electrode particle (c.f. Figures 3b and 3c). For this single axisymmetric electrode, the governing equation of phase p Eq. (12) reduces to

$$\frac{\partial c^p}{\partial t} = \frac{D^p}{r^2}\frac{\partial}{\partial r}\left(r^2 \frac{\partial c^p}{\partial r} - \frac{c^p \Omega^p}{RT} r^2 \frac{\partial \sigma_h^p}{\partial r} \right) \tag{27}$$

The gradient of the hydrostatic stress can be rewritten as

$$\frac{\partial \sigma_h^p}{\partial r} = -\frac{2E^p}{1-\nu^p}\frac{\Omega^p}{9}\frac{\partial c^p}{\partial r} \tag{28}$$

Substituting Eq. (28) into Eq. (27), the final governing equation is obtained,

$$\frac{\partial c^p}{\partial t} = \frac{D^p}{r^2}\frac{\partial}{\partial r}\left(\left(1+\theta^p c^p\right) r^2 \frac{\partial c^p}{\partial r} \right) \tag{29}$$

where $\theta^p = 2E^p(\Omega^p)^2/[9(1-\nu^p)RT]$. Rewrite the dimensionless parameter $\lambda^p = \theta^p c^p = \theta^p c_{max} \cdot c^p/c_{max}$. Considering $c^p/c_{max} \in (0, 1)$, one can expect that the effect of hydrostatic stress depends on the value of λ^p. Define the effective diffusivity $D_{eff}^p = D^p\left(1+\theta^p c^p\right)$, and rewrite Eq. (29) as

$$\frac{\partial c^p}{\partial t} = \frac{1}{r^2}\frac{\partial}{\partial r}\left(r^2 D_{eff}^p \frac{\partial c^p}{\partial r} \right) \tag{30}$$

One can observe that the governing equation could reduce to a similar form to the classical diffusion equation. The effects of hydrostatic stress are effected via a concentration dependent diffusivity. The lithium ion flux is inserted into and extracted from the electrode through the outer surface. So the outer surface is active, while inner surface is inactive. Therefore, the specific form of boundary condition Eq. (14) is

http://dx.doi.org/10.5772/62577

$$-D_{\text{eff}}^{p}\left.\frac{\partial c^{p}}{\partial r}\right|_{r=r_1}=0;\quad -D_{\text{eff}}^{p}\left.\frac{\partial c^{p}}{\partial r}\right|_{r=r_2}=\frac{i_n}{F} \tag{31}$$

Eq. (31) implies that the concentration gradient at the outer surface is inversely proportional to the factor $1+\theta^{p}c^{p}$.

When the concentration at the outer surface reaches the equilibrium value of the α phase, phase transformation begins. Figure 3a illustrates the biphase hollow electrode particle. Combining the diffusion process of two phases, one can obtain the governing equations from Eq. (29),

$$\begin{cases}\dfrac{\partial c^{\alpha}}{\partial t}=\dfrac{1}{r^2}\dfrac{\partial}{\partial r}\left(r^2 D_{\text{eff}}^{\alpha}\dfrac{\partial c^{\alpha}}{\partial r}\right) & r_1\le r\le\xi\\ \dfrac{\partial c^{\beta}}{\partial t}=\dfrac{D^{\beta}}{r^2}\dfrac{\partial}{\partial r}\left(r^2 D_{\text{eff}}^{\beta}\dfrac{\partial c^{\beta}}{\partial r}\right) & \xi\le r\le r_2\end{cases} \tag{32}$$

For the hollow spherical particles, the governing equation of the moving interface Eq. (17) reduces to

$$\left(c_{eq}^{\alpha}-c_{eq}^{\beta}\right)\frac{d\xi}{dt}=D_{\text{eff}}^{\beta}\frac{\partial c^{\beta}}{\partial r}-D_{\text{eff}}^{\alpha}\frac{\partial c^{\alpha}}{\partial r} \tag{33}$$

where $d\xi/dt$ is the moving velocity of the phase interface. Note that the contributions of θ^{α} and θ^{β} to the movement of phase interface have been ignored in the previous work. One can regard the current version of moving interface equation as the same as the one in [33] but replacing the constant diffusivity D^{p} with an effective diffusivity D_{eff}^{p}.

The concentrations at two sides of the interface are equal to their own equilibrium values, i.e.,

$$c^{\alpha}\Big|_{r=\xi}=c_{eq}^{\alpha};\quad c^{\beta}\Big|_{r=\xi}=c_{eq}^{\beta} \tag{34}$$

At this stage, the α phase satisfies the boundary condition at the inner surface, while β phase satisfies the boundary condition at the outer one, i.e.,

$$-D_{\text{eff}}^{\alpha}\left.\frac{\partial c^{\alpha}}{\partial r}\right|_{r=r_1}=0;\quad -D_{\text{eff}}^{\beta}\left.\frac{\partial c^{\beta}}{\partial r}\right|_{r=r_2}=\frac{i_n}{F} \tag{35}$$

During the phase transformation process, the α phase gradually transforms into β phase, and the phase interface moves inward. When the phase transformation finishes, the phase interface reaches the inner surface ($\xi = r_1$), and only β phase is left in the electrode particle (c.f. Figure 3c).

Initially, the lithium ions are uniformly distributed inside the electrode particle, i.e.,

$$c^p\left(r, t=0\right) = c^0, \quad r \in \left[r_1, r_2\right] \tag{36}$$

The beauty of the formulation for the hollow spherical particle is that the governing equations Eqs. (29), (32), and (33) are decoupled from the stress field explicitly. This implies that one can directly compute the concentration field by using Eqs. (29)–(36) instead of solving a fully coupled system, and then calculate the stress field using Eqs. (22)–(26) at each step.

4.2. Concentration and stress fields

Section 4.1 provides the model to compute concentration and stress fields. The effect of hydrostatic stress is coupled into governing equation Eq. (32), and the surface/interface stress are effected via Eq. (23) and (26). To reveal the interactions between stress profile and phase transformation, a hollow spherical electrode particle is analyzed, for example. The inner and outer radii of electrode particle are 10 and 20 μm, and the particle is discharged under 10 A/m^2 currency density. Here and in the following, $LiCoO_2$ is used as the electrode material unless otherwise specified because it is the mostly reported electrode material with phase transformation phenomenon and most widely used in industry. The material properties of $LiCoO_2$ are provide in [32].

4.2.1. Concentration field

The concentration field of the electrode particle at the three stages are calculated (c.f. Figure *4*). At the first stage, there is α phase only. **Figure 4a** illustrates the lithium ions' concentration at different time in this stage. Observations show that the concentration increases monotonically with *r* from the inner surface to the outer one. Because of the inward flux at the outer surface, the concentration keeps increasing with time. However, the concentration gradient decreases with time. This is consistent with Eq. (*31*) which implies that the concentration gradient is inversely proportional to the factor $1 + \theta c$. Therefore, the concentrations at the inner and outer surfaces are significantly different at 50 seconds, but close to each other at 500 seconds. The first stage finishes at 2106.5 seconds, when the concentration at the outer surface reaches c_{eq}^{α}, and the phase transformation begins.

When the phase transformation happens, a phase interface appears between the $\boldsymbol{\alpha}$ and $\boldsymbol{\beta}$ phases. Driven by the interface flux jump, the phase interface gradually moves towards the inner surface. **Figure 4b** illustrates the concentration distribution when the phase interface is at different positions. The concentrations of the two phases at the interface equal their own equilibrium values, i.e., c_{eq}^{α} and c_{eq}^{β}. Because $c_{eq}^{\alpha} = 0.75\, c_{max}$ and $c_{eq}^{\beta} = 0.97 c_{max}$, a sharp concentration jump is observed at the phase interface. Similar to the first stage, the concentration increases

with time during the phase transformation. However, under the effect of concentration discontinuity, the concentration gradient also increases with time. This is because the concentration increasing at the outer surface is slower than the movement of phase interface. When the phase transformation finishes, the concentration is c_{eq}^{β} at the inner surface, while close to c_{max} at the outer surface.

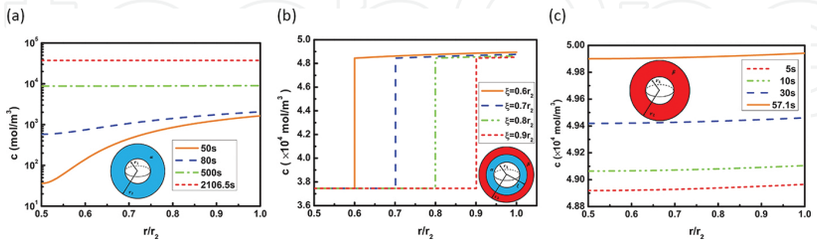

Figure 4. Concentration distribution of the electrode particle: (a) with α phase only; (b) with both α and β phases; (c) with β phase only (some data are reproduced from [47]).

To address the interactions between phase transformation and stress field, one can first investigate the effect of hydrostatic stress on the phase transformation. Please recall that the governing equation of the phase interface is modified to include the gradient of hydrostatic stress. Table 1 lists the time it needs for the phase interface to arrive the positions illustrated in Figure 4b. Compared with the conventional equations without considering the effect of hydrostatic stress, the moving speed of phase interface is much faster, which implies that the time during the phase transformation stage is overestimated by the previous models [33]. This is because the factor $(1+\boldsymbol{\theta c})$ significantly increases the flux jump at the interface, i.e., the driven force of interface movement. In other words, one can conclude that the effect of hydrostatic stress can significantly accelerate the phase transformation.

Position	Without hydrostatic stress	With hydrostatic stress
0.9 r_2	23,500 s	171 s
0.8 r_2	44,950 s	328 s
0.7r_2	61,210 s	452 s
0.6r_2	73,700 s	550 s

Table 1. Time needed for the movement of phase interface.

When the phase interface arrives at the inner surface, the phase transformation ends and the third stage begins. There is β phase only in the electrode at this stage. The concentration distribution at different time is illustrated in **Figure 4c**. Because the concentration at outer surface has been close to c_{max} at the end of second stage, the third stage only takes about 57 seconds. Similar to the first stage, concentration increases with time while its gradient decreases with time. In the end, the concentration increases with r, and is close to c_{max}

everywhere. Please note this is only the end of galvanostatic process, which is followed by potentiostatic operation to fully discharge the battery.

4.2.2. Stress profile

Lithium ion is non-uniformly distributed in the electrode and induces stresses. The stress field of a single phase electrode particle has been investigated by many researchers [18, 21, 35, 36], while the stress field of the biphase one is still unknown. Eq. (22) implies that the stress fields are explicitly related to the concentration field. One can expect the interface concentration discontinuity to have a significant influence on the stress field, which is illustrated in **Figure 5**. The constant surface stress $\tau^0 = 1 J/m^2$ and surface modulus $K^s = 5 N/m$, unless otherwise specified [11]. The radial stress of the single phase electrode particle monotonically increases/decreases in the discharging/charging process [14, 18]. But the radial stress of this biphase particle increases from the inner surface to the phase interface and decreases from the interface to the outer surface. The stresses predicted from the present model are compared with those from the one without considering surface/interface effect. Without considering the surface effect, radial stress is zero at the surfaces because Eq. (26) reduces to the traction free boundary condition. Under the effect of surface stress, the radial stress is positive at the inner surface, and negative at the outer one. This implies that the electrode particle boundaries can still under tension or compression though no external load is applied. Without considering the interface effect, the radial stress is continuous at the interface since Eq. (23) reduces to the continuity condition and is automatically satisfied. Under the interface effect, a positive stress jump is observed at the interface. Please note the surface/interface effects are highlighted for this hollow biphase particle, due to its double surfaces and sharp interface.

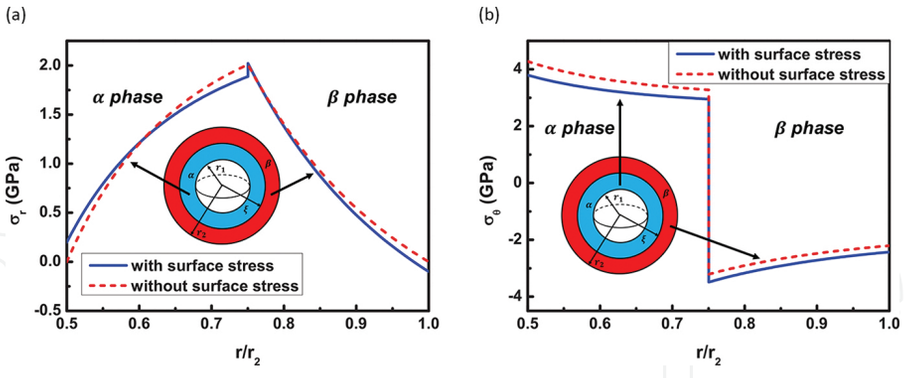

Figure 5. Stress field in the biphase electrode: (a) radial stress; (b) hoop stress (some data are reproduced from [47]).

Hoop stress is the driven force for the propagation of manufacture-induced imperfection. Therefore, hoop stress is more important in the stress analysis of electrode particles. One can observe that the hoop stress decreases from the inner surface to the outer one in the α phase. With a jump at the interface, the hoop stress changes from positive into negative value. It increases from phase interface to the outer surface. Compared to that of radial stress, the discontinuity of hoop stress at the interface is high. The reason for this high discontinuity is that the hoop stress is directly related to the interface discontinuous concentration. Therefore,

the effect of the phase transformation on hoop stress is worth more attention. By comparison, one can find that the surface/interface effect on hoop stress is much smaller.

The interactions between stress fields and phase transformation is systematically investigated in the above. One can conclude that the hydrostatic stress could accelerate the phase transformation and the time during phase transformation is overestimated by the conventional model without considering the effect of hydrostatic stress [33]. Moreover, the during the phase transformation, there is a sharp phase interface. The phase interface induced discontinuity in both radial and hoop stresses, and made the stress field in the electrode significantly higher. In summary, the phase transformation increases the stress field and therefore threatens the safety of electrode particle. But the hydrostatic stress could help the electrode to finish the phase transformation faster, and is important to avoid the failure of electrode particle.

5. Electrode geometry analysis

A key concept to avoid the stress-induced electrode failure is to find an optimal electrode, in which the stress is lower. In order to optimize the electrode, size and shape of the electrodes are two major topics to investigate. Different sized electrodes are studied during the last decades and considerable efforts are put into searching electrodes with optimal shapes, and researchers have tested multiple shapes [13, 34–36, 40–42]. However, those work mainly focus on the investigation of single phase solid electrodes. Hollow particle, with a unique doubled surface area, core-shell structure and large internal void, has great potentials in applications of lithium-ion batteries [42]. In Section 4, the concentration and stress profile of hollow electrode particles are analyzed. This section will study the size and shape effects of this hollow spherical particles.

5.1. Size effect

Size effect implies the dependence of the stress fields on the size of electrode particles, which has been investigated by researchers [11, 14, 18]. They conclude that larger particles lead to higher concentration gradient and induce higher stress. However, the model used in the above work is fairly simple. In the present model, the size effect can interact with the effects of hydrostatic stress and interface/surface stress, and have more complicated behaviors. To investigate this effect, a cross scale analysis is presented here, with particle size ranging from 10 nm to 20 μm and being discharged under 10 A/m^2 are simulated. The inner radii are half of the outer ones for these electrode particles.

5.1.1. Hydrostatic stress-induced size effect

Section 4 highlights the effect of hydrostatic stress on concentration and stress. In what follows, we will discuss the dependence of its effect on electrode size. **Figures 6a** illustrates the maximum hoop stresses of different sized electrode particles, when the concentration at the outer surface reaches c_{eq}^{α}. The stress fields with/without considering the effect of hydrostatic

stress are compared. The stress fields predicted by two models are almost the same for the nanoelectrode particles, but are significantly different for the micro electrode particles. Without the effect of σ_h, large concentration gradient exists in large electrode particles, which induces the stress as high as 160 MPa. However, the stress field is not that high in reality. This is because σ_h can lower the concentration gradient and, therefore lower the stress fields. One can also explain the effect of σ_h as follows: the "effective" inward flux at outer surface $D\partial c/\partial r = i_n/F(1 + \theta c)$ decreases with c, which is equivalent to the case that the battery is discharged in a lower currency density. And it is well known that the stress of the electrode particle is lower when discharged under a lower currency density. Therefore, one can conclude that the effect of σ_h is necessary in stress predictions for the micro particles, but can be neglected for the nanoparticles.

5.1.2. Surface stress-induced size effect

In the community of solid mechanics, the surface stress-induced size effect is widely observed [45, 51, 52]. In 2008, Cheng et al. [11] introduces the surface stress effect to stress analysis of nano $LiMn_2O_4$ solid electrode particles in lithium-ion batteries. Here the size effect with surface stress is presented for the hollow spherical electrodes. We analyze the surface stress-induced size effect in the first stage of discharging process, since there is only α phase left and the effect of surface stress and phase transformation is decoupled. The maximum hoop stress $\sigma_{\theta max}$ of different-sized electrode particles are computed (c.f. **Figure 6b**). When the electrode particle is in micro size, the stresses predicted by the model with/without surface stress effect are almost the same. $\sigma_{\theta max}$ increases with particle size and reaches around 200 MPa when the particle size is 10 μm. However, a great difference is observed when the electrode particle size is nanoscale. Without considering the surface stress, $\sigma_{\theta max}$ is close to zero, which implies the whole particle is at the stress free state. But the stress predicted by the model with surface effect shows that the $\sigma_{\theta max}$ becomes negative, whose absolute values is large. This means the whole particle is under compression, which is important for the electrodes with flaw or small cracks, because the compression can stop the growth of these cracks. Therefore, the surface stress has to be considered in predicting the stress field of nanoelectrode particles.

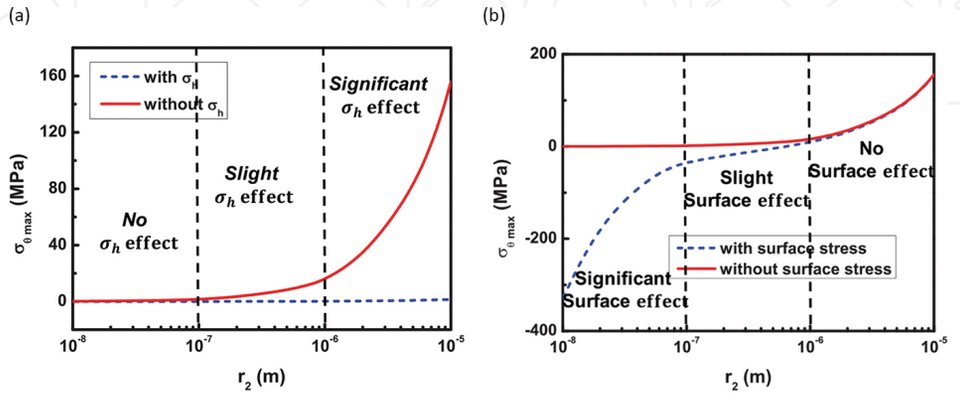

Figure 6. Variation of $\sigma_{\theta max}$ with size of electrode particles: (a) under effect of hydrostatic stress; (b) under effect of surface stress (some data are reproduced from [47]).

http://dx.doi.org/10.5772/62577

5.1.3. Interface stress-induced size effect

Although the surface effect of electrode particles has been reported for several years [11], the interface stress is not considered until the recent work of the authors [47]. In fact, for hollow electrode particles, the surface stress at the inner and outer surfaces are just special cases of interface stress Eq. (3). Since the size effect of surface stresses is reported above, the size effect due to interface stresses is expected.

Figures 7 illustrates the stress fields of different sized biphase electrode particles, that are discharged under 10 A/m^2 currency density. For the micro electrode particle, the interface stress is not significant and the discontinuity of σ_r at phase interface is small. However, when the size of electrode reaches nanoscale, the interface stress is much higher, which leads to a higher stress discontinuity at the phase interface. Recall that before the phase transformation, the nanoelectrode particles is under compression due to the surface stress. But it is under tension due to the high stress discontinuity. Because the tensional stress may drive the existing crack to propagate, the biphase stage is the most dangerous. Furthermore, stresses increase by more than 200 times in this stage, and threaten the safety of electrodes.

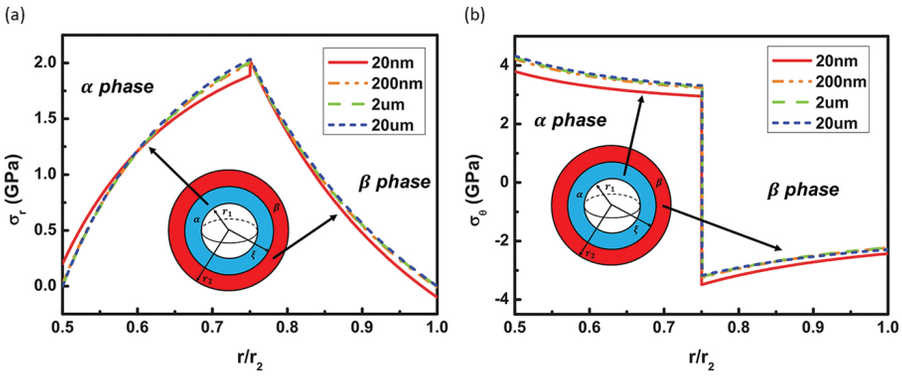

Figure 7. Variation of stress fields with sizes of electrodes: (a) σ_r; (b) σ_θ (some data are reproduced from [47]).

In summary, hydrostatic stress, surface stress, and interface stress can all induce size effect. The effect of hydrostatic stress increases with particle size while the effects of surface and interface stresses decrease with particle size. This is because the hydrostatic stress is inserted into bulk equations while the surface/interface stress is considered in the surface/interface equations. The ratio of surface/interface over volume decreases with the particle size, so do the effects of surface/interface stresses.

5.2. Shape effect

Because of its better cyclability, higher rate capability, and less capacity degradation compared to the solid sphere electrodes [46, 48, 49], hollow electrode particle attracts wide research attention. The structural feature of hollow particles, i.e., shape effect, can be characterize by a parameter $\zeta = r_1/r_2$. The hollow sphere could reduce to solid ones when $\zeta = 0$ ($r_1 = 0$), and become a thin shell when $\zeta \approx 1$ ($r_1 \approx r_2$). The shape effect on the mechanical and electrochemical properties of hollow electrode particles are systematically investigated in the following.

5.2.1. Shape effect on stress

The maximum and minimum hoop stresses of hollow particles with different ζ but same volume are compared (**Figure 8a**). To highlight this shape effect, no interface/surface and hydrostatic stresses are considered here. One can observe that the absolute values of maximum and minimum hoop stresses both decrease with ζ. The stress of the particles with $\zeta = 0.05$ is even 20 times more than that with $\zeta = 0.95$. The advantages of hollow electrode particles will be strengthened in thin shell structure, and zero stress state is expected when $\zeta \to 1$. Stress profiles are calculated for the hollow particles with same outer radius 13.82 μm, but with different inner radii. The maximum and minimum hoop stresses ($\sigma_{\theta max}$ and $\sigma_{\theta min}$) are illustrated in **Figure 8b**. Observations show that the absolute values of $\sigma_{\theta max}$ and $\sigma_{\theta min}$ decrease with ζ. In other words, the stresses decrease with the shell thickness of hollow particles. When $\zeta \to 1$, the thickness is close to zero and the hollow particle approaches a single thin layer shell in which no concentration gradient or stress exist.

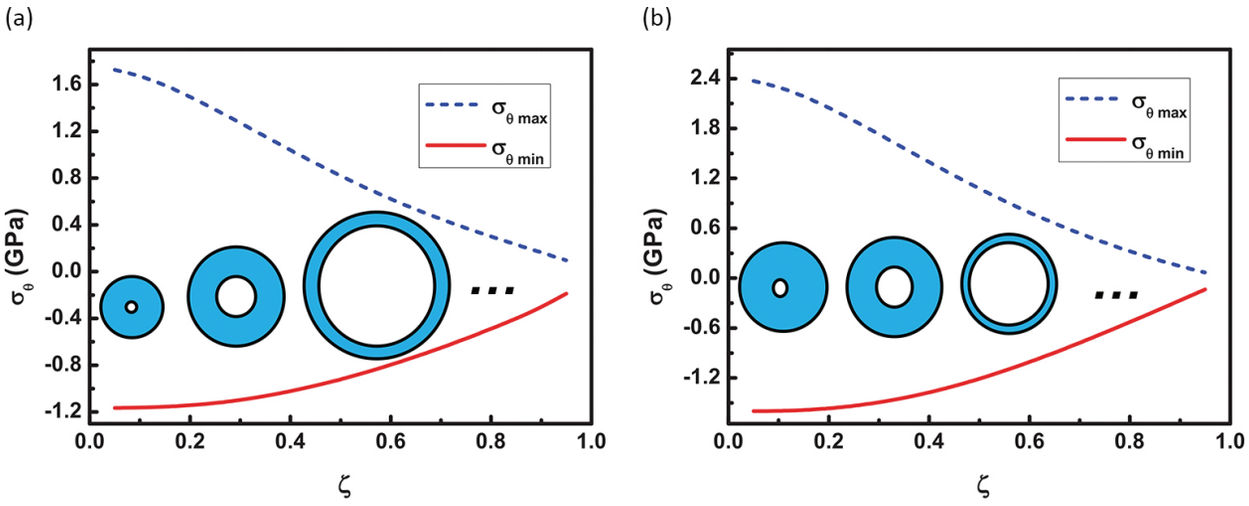

Figure 8. Maximum and minimum hoop stresses: (a) different sizes with same volume; (b) different volumes with same sizes (some data are reproduced from [47]).

In conclusion, the hollow structure electrodes can significantly reduce the stress field of electrode. The hoop stress decreases with the thickness of the shell. Furthermore, because the tensional hoop stress is the driven force of crack growth in the electrode, hollow structure can help to lower the failure possibility of lithium ion batteries.

5.2.2. Shape effect in efficiency

At the end of galvanostatic process, there is some residual capacity. The residual lithium will be in waste without the potentiostatic operation. To characterize the effective capacity of the battery, a variable η is defined as the ratio of effective capacity to total capacity,

http://dx.doi.org/10.5772/62577

$$\eta = \frac{\mathrm{Cap_t} - \mathrm{Cap_{re}}}{\mathrm{Cap_t}} \tag{37}$$

where $\mathrm{Cap_t}$ and $\mathrm{Cap_{re}}$ are total and residual capacities. Please note that $\eta \le 1$ since $\mathrm{Cap_{re}} \ge 0$. By performing the potentiostatic charging, the battery gets fully charged/discharged, i.e., $\mathrm{Cap_{re}}$ can reduce to 0 and η will reach 1.

For this special electrode, the total capacity is

$$\mathrm{Cap_t} = \frac{4\pi}{3} Q\rho\Omega c_{max}(r_2^3 - r_1^3) \tag{38}$$

where Q is the theoretical capacity of the electrode material. The residual capacity of the electrode particle is

$$\mathrm{Cap_{re}} = 4\pi Q\rho\Omega \int_{r_1}^{r_2} cr^2 dr \tag{39}$$

Substitution of Eq. (39) into Eq. (38) yields

$$\eta = 1 - \frac{3\int_{r_1}^{r_2} cr^2 dr}{c_{\max}\left(r_2^3 - r_1^3\right)} \tag{40}$$

$Li_xMn_2O_4$ is taken as an example to analyze the efficiency of the electrodes, whose material properties are provided in [14]. Variation of η with ζ is illustrated (Figure 9). One can observe that η increases with ζ, and approaches 1 when ζ is close to 1. This implies that the effective capacity can be high enough without potentiostatic charging as long as the shell is thin enough.

The particle sizes and charging densities have significant influence on the stress profile of electrode particles. In what follows, their effects on the efficiency are investigated. **Figure 9a** illustrates the dependence of efficiency on charging currency density when the electrode particles have the same size $r_2 = 20$ μm. Observations show that η becomes higher when the electrode is charged under lower currency density. The efficiency η is above 96% regardless of ζ , when $i_n = 5$ A/m^2. The efficiencies of different-sized electrode particles are compared in **Figure 9b**. The particles are all charged under the same currency density $i_n = 20$ A/m^2 . One can observe that smaller electrode particles have higher efficiency. When the electrode particle is small (i.e. $r_2 = 5$ μm), the efficiency is above 96%.

In summary, the efficiency of electrode particle depends on particle size, shell thickness, and charging currency density. High effective capacity can be obtained by using thin shell hollow particle, small electrode particle, and low currency density.

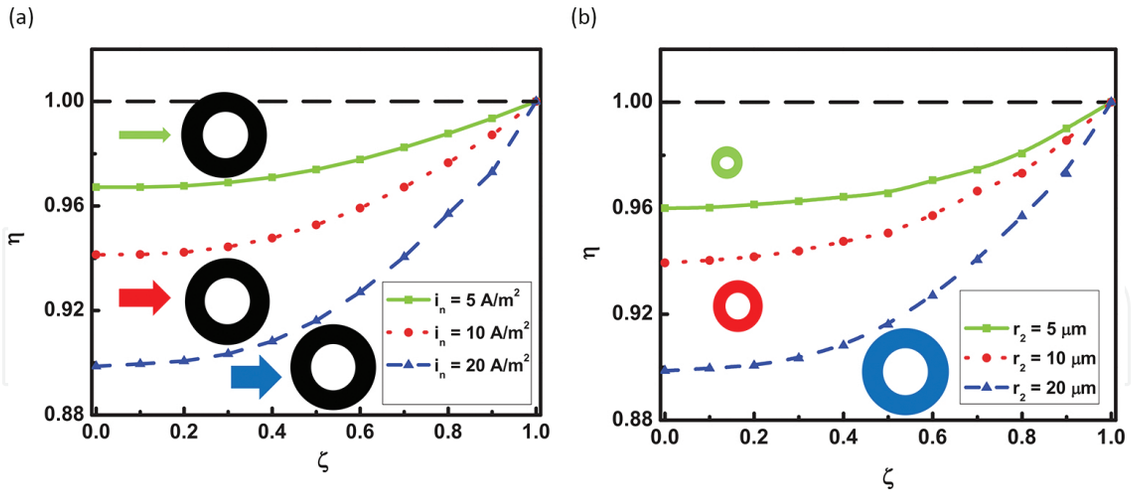

Figure 9. Variation of η with ζ: (a) different currency densities; (b) different sizes (some data are reproduced from [47]).

The size and shape effect of hollow spherical particles are systematically investigated above. The size effect is observed for the hydrostatic stress, surface stress, and interface stress, which implies that hydrostatic stress is important in predicting the stress of micro particles while surface and interface stresses are essential in computing the stress fields of nanoparticles. The advantages of hollow electrode particles are highlight in significantly reducing the stress and increasing the efficiency. In summary, hollow structure particle can significantly improve the mechanical and electrochemical properties and is a good candidate for the optimal electrode particle.

6. Conclusions

This chapter reviews the models on stress analysis of electrode particles in lithium-ion batteries, and then provides an electrochemo-mechanical framework to model the concentration and stress of an electrode with arbitrary geometry. The hydrostatic stress and surface/interface stress are considered. The interactions between phase transformation and stress profile are investigated. The equations are then reformulated for the specific hollow spherical electrode particles. Conclusions are summarized as follows:

1. The interaction between stress fields and phase transformation is fully addressed. Under the effect of hydrostatic stress, the phase transformation process is much faster, which implies the time of phase transformation is overestimated in previous publications. Due to the existence of phase interface, the stress becomes discontinuous at the interface. The stresses filed of the whole electrode is much larger in the biphase stage.

2. The size and shape effects for hollow spherical particle are investigated. Through a cross-scale analysis, we conclude that hydrostatic stress, surface stress and interface stress can all induce size effect. Hydrostatic stress is important in predicting the stress of micro particles while surface and interface stresses are essential in computing the stress fields of nanoparticles.

3. The shape effect of the hollow electrode particle is analyzed, which highlights its structural advantages. One can find that the stress field highly depends on ζ ($=r_1/r_2$). The maximum hoop stress decreases with ζ. When ζ is close to 1, the stress is approaching zero. A variable η, to characterize the efficiency (ratio of effective capacity over total capacity) of battery is defined. η also decreases with ζ. When the thickness of hollow electrode particle is small enough, η is close to 1. Therefore, the hollow particle is a good candidate for the optimal electrode particle.

This chapter presents an electrochemo-mechanical framework to accurate predict the stress profile in the electrode particles with different sizes and geometries. The proposed framework considers different effects simultaneously, and quantitatively compares their contributions. This chapter also proposes an optimal electrode particle, i.e., the hollow spherical particle, and systematically analyzes its size and shape effects. Therefore, the present chapter is helpful for the material and structure design of electrode.

Acknowledgements

This work is sponsored by the Alexander von Humboldt (AvH) foundation through project 'Mechanics theory of materials with complex surfaces and its applications'; Huiling Duan appreciates the support of following agencies: Major State Basic Research Development Programme of China, National Natural Science Foundation of China.

Author details

Yingjie Liu[1] and Huiling Duan[2*]

*Address all correspondence to: hlduan@pku.edu.cn

1 Computational Mechanics Lab, Department of Civil and Environmental Engineering, Duke University, Durham, NC, USA

2 State Key Lab for Turbulence and Complex System, Department of Mechanics and Engineering Science, Peking University, Beijing, PR China

References

[1] Baker DR, Verbrugge MW. The role of charge separation in the response of electrochemical systems. Proc. R. Soc. Lond. A. 2002;454,1805–1829. (DOI:10.1098/rspa.1998.0233)

[2] Yi Y-B, Sastry AM. Analytical approximation of the percolation threshold for overlapping ellipsoids of revolution. Proc. R. Soc. Lond. A. 2004;460,2353–2380. (DOI:10.1098/rspa.2004.1279)

[3] Wu Y, Pasero D, Mc Cabe EE, Matsushima Y, West AR. Partial cation-order and early-stage, phase separation in phase W, $Li_xCo_{1-x}O$: $0.07 \leq x \leq 0.24 - 0.3$. Proc. R. Soc. A. 2009;465,1829–1841. (DOI:10.1098/rspa.2008.0489)

[4] Mc Kenna KP, Shluger AL. Electron and hole trapping in polycrystalline metal oxide materials. Proc. R. Soc. A. 2011;467,2043–2053. (DOI:10.1098/rspa.2010.0518)

[5] Maksimchuk NV, Zalomaeva OV, Skobelev IY, Kovalenko KA, Fedin VP, Kholdeeva OA. Metal-organic frameworks of the MIL-101 family as heterogeneous single-site catalysts. Proc. R. Soc. A. 2012;468,2017–2034. (DOI:10.1098/rspa.2012.0072)

[6] Chen CQ, et al. Perspectives in mechanics of heterogeneous solids. Acta Mech. Solida Sin. 2011;24,1–26. (DOI:10.1016/S0894-9166(11)60007-4)

[7] Christensen J, Newman J. A mathematical model of stress generation and fracture in lithium manganese oxide. J. Electrochem. Soc. 2006;153,A1019–A1030. (DOI: 10.1149/1.2185287)

[8] Jang YI, Huang BY, Wang HF, Sadoway DR, Ceder G, Chiang YM, Liu H, Tamura H. $LiAlyCo_{1-y}O_2$ (R_{3m}) intercalation cathode for rechargeable lithium batteries. J. Electrochem. Soc. 1999;146,862–868. (DOI:10.1149/1.1391693)

[9] Wang HF, Jang Y-II, Huang B, Sadoway DR, Chiang Y-M. Electron microscopic characterization of electrochemically cycled $LiCoO_2$ and $Li(Al,Co)O_2$ battery cathodes. J. Power Sources. 1999;81–82,594–598. (DOI:10.1016/S0378-7753(99)00108-1)

[10] Gabrisch H, Wilcox J, Doeff MM. TEM study of fracturing in spherical and plate-like $LiFePO_4$ particles. Electrochem. Solid State Lett. 2008;11,A25–A29. (DOI: 10.1149/1.2826746)

[11] Cheng Y-T, Verbrugge MW. The influence of surface mechanics on diffusion induced stresses within spherical nanoparticles. J. Appl. Phys. 2008;104,083521. (DOI: 10.1063/1.3000442)

[12] Cheng Y-T, Verbrugge MW. Evolution of stress within a spherical insertion electrode particle under potentiostatic and galvanostatic operation. J. Power Sources. 2009;190,453–460. (DOI:10.1016/j.jpowsour.2009.01.021)

[13] Lu B, Song YC, Guo ZS, Zhang JQ. Analysis of delamination in thin film electrodes under galvanostatic and potentiostatic operations with Li-ion diffusion from edge. Acta. Mech. Sinica. 2013;29,348–356. (DOI: 10.1007/s10409-013-0038-x)

[14] Woodford WH, Chiang Y-M, Carter WC. 'Electrochemical shock' of intercalation electrodes: a fracture mechanics analysis. J. Electrochem. Soc. 2010;157,A1052–A1059. (DOI:10.1149/1.3464773)

[15] Hu YH, Zhao XH, Suo ZG. Averting cracks caused by insertion reaction in lithium-ion batteries. J. Mater. Res. 2010;25,1007–1010. (DOI:10.1557/JMR.2010.0142)

[16] Zhao KJ, Wang WL, Gregoire J, Pharr M, Suo ZG, Vlassak JJ, Kaxiras E. Lithium-assisted plastic deformation of silicon electrodes in lithium-ion batteries: a first-principles theoretical study. Nano Lett. 2011;11,2962–2967. (DOI:10.1021/nl201501s)

[17] Zhang XC, Sastry AM, Shyy W. Intercalation-induced stress and heat generation within single lithium-ion battery cathode particles. J. Electrochem. Soc. 2008;155,A542–A552. (DOI:10.1149/1.2926617)

[18] Zhang XC, Shyy W, Sastry AM. Numerical simulation of intercalation-induced stress in li-ion battery electrode particles. J. Electrochem. Soc. 2007;154,A910–A916. (DOI: 10.1149/ 1.2759840)

[19] Park J, Lu W, Sastry AM. Numerical simulation of stress evolution in lithium manganese dioxide particles due to coupled phase transition and intercalation. J. Electrochem. Soc. 2011;158,A201–A206. (DOI:10.1149/1.3526597)

[20] Park J, Seo JH, Plett G, Lu W, Sastry AM. Numerical simulation of the effect of the dissolution of $LiMn_2O_4$ particles on li-ion battery performance. Electrochem. Solid-State Lett. 2011;14,A14–A18. (DOI:10.1149/1.3516619)

[21] Cheng Y-T, Verbrugge MW. Application of hasselman's crack propagation model to insertion electrodes. Electrochem. Solid-State Lett. 2010;13,A128–A131. (DOI: 10.1149/1.3455179)

[22] Zhao KJ, Pharr M, Vlassak JJ, Suo ZG. Fracture of electrodes in lithium-ion batteries caused by fast charging. J. Appl. Phys. 2010;108,073517. (DOI:10.1063/1.3492617)

[23] Grantab R, Shenoy VB. Location- and orientation-dependent progressive crack propagation in cylindrical graphite electrode particles. J. Electrochem. Soc. 2011;158,A948–A954. (DOI:10.1149/1.3601878)

[24] Haftbaradaran H, Gao HJ, Curtin WA. A surface locking instability for atomic intercalation into a solid electrode. Appl. Phys. Lett. 2010;96,091909. (DOI: 10.1063/1.3330940)

[25] Haftbaradaran H, Song J, Curtin WA, Gao HJ. Continuum and atomistic models of strongly coupled diffusion, stress, and solute concentration. J. Power Sources. 2011;196,361–370. (DOI:10.1016/j.jpowsour.2010.06.080)

[26] Hu YH, Zhao XH, Suo ZG. Averting cracks caused by insertion reaction in lithium-ion batteries. J. Mater. Res. 2010;25,1007–1010. (DOI:10.1557/JMR.2010.0142)

[27] Zhao KJ, Wang WL, Gregoire J, Pharr M, Suo ZG, Vlassak JJ, Kaxiras E. Lithium-assisted plastic deformation of silicon electrodes in lithium-ion batteries: a first-principles theoretical study. Nano Lett. 2011;11,2962–2967. (DOI:10.1021/nl201501s)

[28] Nytén A, Abouimrane A, Armand M, Gustafsson T, Thomas JO. Electrochemical performance of Li_2FeSO_4 as a new li-battery cathode material. Electrochem. Commun. 2005;7,156–160. (DOI:10.1016/j.elecom.2004.11.008)

[29] Ramesh TN, Lee KT, Ellis BL, Nazar LF. Tavorite lithium iron fluorophosphate cathode materials: phase transition and electrochemistry of $LiFePO_4F$-Li_2FePO_4F. Electrochem. Solid-State Lett. 2010;13,A43–A47. (DOI:10.1149/1.3298353)

[30] Shin HC, Pyun SI. An investigation of the electrochemical intercalation of lithium into a Li1−δ CoO_2 electrode based upon numerical analysis of potentiostatic current transients. Electrochim. Acta. 1999;44,2235–2244. (DOI:10.1016/S0013-4686(98)00340-5)

[31] Shin HC, Pyun SI. The kinetics of lithium transport through Li1−δ CoO_2 by theoretical analysis of current transient. Electrochim. Acta. 1999;45,489–501. (DOI:10.1016/S0013-4686(99)00270-4)

[32] Zhang Q, White RE. Moving boundary model for the discharge of a $LiCoO_2$ electrode. J. Electrochem. Soc. 2007;154,A587–A596. (DOI:10.1149/1.2728733)

[33] Renganathan S, Sikha G, Santhanagopalan S, White RE. Theoretical analysis of stresses in a lithium ion cell. J. Electrochem. Soc. 2010;157,A155–A163. (DOI:10.1149/1.3261809)

[34] Li JC-M. Physical chemistry of some microstructural phenomena. MTA. 1978;9,1353–1380. (DOI:10.1007/BF02661808)

[35] Hao F, Fang DN. Diffusion-induced stresses of spherical core-shell electrodes in lithium- ion batteries: the effects of the shell and surface/interface stress. J. Electrochem. Soc. 2013;160,A595–A600. (DOI:10.1149/2.054304jes)

[36] Hao F, Fang DN. Tailoring diffusion-induced stresses of core-shell nanotube electrodes in lithium-ion batteries. J. Appl. Phys. 2013;113,013507. (DOI:10.1063/1.4772963)

[37] Deshpande R, Cheng Y-T, Verbrugge MW. Modeling diffusion-induced stress in nanowire electrode structures. J. Power Sources. 2010;195,5081–5088. (DOI:10.1016/j.jpowsour. 2010.02.021)

[38] Xiao X, Liu P, Verbrugge MW, Haftbaradaran H, Gao HJ. Improved cycling stability of silicon thin film electrodes through patterning for high energy density lithium batteries. J. Power Sources. 2011;196,1409–1416. (DOI:10.1016/j.jpowsour.2010.08.058)

[39] Lu B, Song YC, Guo ZS, Zhang JQ. Modeling of progressive delamination in a thin film driven by diffusion-induced stresses. Int. J. Solids Struct. 2013;50,2495–2507. (DOI: 10.1016/j.ijsolstr.2013.04.003)

[40] Zhang JQ, Lu B, Song YC, Ji X. Diffusion induced stress in layered Li-ion battery electrode plates. J. Power Sources. 2012;209,220–227. (DOI:10.1016/j.jpowsour. 2012.02.104)

[41] Bhandakkar TK, Gao HJ. Cohesive modeling of crack nucleation under diffusion induced stresses in a thin strip: implications on the critical size for flaw tolerant battery electrodes. Int. J. Solids Struct. 2010;47,1424–1434. (DOI:10.1016/j.ijsolstr.2010.02.001)

[42] Bhandakkar TK, Gao HJ. Cohesive modeling of crack nucleation in a cylindrical electrode under axisymmetric diffusion induced stresses. Int. J. Solids Struct. 2011;48,2304–2309. (DOI:10.1016/j.ijsolstr.2011.04.005)

[43] Keng PY, et al. Colloidal polymerization of polymer-coated ferromagnetic nanoparticles into cobalt oxide nanowires. ACS Nano. 2009;3,3143–3157. (DOI:10.1021/nn900483w)

[44] Duan HL, Wang J, Huang ZP, Zhong Y. Stress fields of a spheroidal inhomogeneity with an interphase in an infinite medium under remote loadings. Proc. R. Soc. A. 2005;461,1055–1080. (DOI:10.1098/rspa.2004.1396)

[45] Duan HL, Weissmueller J, Wang Y. Instabilities of core-shell heterostructured cylinders due to diffusions and epitaxy: spheroidization and blossom of nanowires. J. Mech. Phys. Solids. 2008;56,1831–1851. (DOI:10.1016/j.jmps.2007.11.009)

[46] Yao Y, Mc Dowell MT, Ryu I, Wu H, Liu N, Hu LB, Nix WD, Cui Yi. Interconnected silicon hollow nanospheres for lithium-ion battery anodes with long cycle life. Nano Lett. 2011;11,2949–2954. (DOI:10.1021/nl201470j)

[47] Liu YJ, Lv PY, Ma J, Bai RB, Duan HL. Stress fields in hollow coreshell spherical electrodes of lithium ion batteries. Proc. R. Soc. Lond. A. 2014;470,20140299. (DOI: 10.1098/rspa.2014.0299)

[48] Yoon S, Manthiram A. Hollow Core-Shell mesoporous TiO_2 spheres for lithium ion storage. J. Phys. Chem. C. 2011;115, 9410–9416. (DOI:10.1021/jp1123184)

[49] Koo B, Xiong H, Slater MD, Prakapenka VB, Balasubramanian M, Podsiadlo P, Johnson CS, Rajh T, Shevchenko EV. Hollow iron oxide nanoparticles for application in lithium ion batteries. Nano Lett. 2012;12, 2429–2435. (DOI:10.1021/nl3004286)

[50] Lu, B., Song, Y. C., Guo, Z. S., Zhang, J. Q. Modeling of progressive delamination in a thin film driven by diffusion-induced stresses. Int. J. Solids Struct. 2013;50, 2495–2507. (DOI:10.1016/j.ijsolstr.2013.04.003)

[51] Duan HL, Wang J, Huang ZP, Karihaloo BL. Eshelby formalism for nano- inhomogeneities. Proc. R. Soc. A. 2005;461, 3335–3353. (DOI:10.1098/rspa.2005.1520)

[52] Weissmüller J, Duan HL, Farkas D. Deformation of solids with nanoscale pores by the action of capillary forces. Acta Mater. 2010;58, 1–13. (DOI:10.1016/j.actamat. 2009.08.008)

[53] Yvonnet J, Le-Quang H, He QC. An XFEM/level set approach to modeling surface/interface effects and to computing the size-dependent effective properties of nanocomposites. Comput. Mech. 2008;42, 119–131. (DOI:10.1007/s00466-008-0241-y)

[54] Yvonnet J, Le-Quang H, Toulemonde C, He QC. Thermo-mechanical modelling of materials containing micro/nano inclusions with imperfect interfaces. Int. J. Mater. Form. 2008;1, 1139–1142. (DOI:10.1007/sl2289-008-0181-2)

[55] Wang WL, Lee S, Chen JR. Effect of chemical stress on diffusion in a hollow cylinder. J. Appl. Phys. 2002;91, 9584–9590. (DOI:10.1063/1.1477624)

[56] Fischer FD, Svoboda J. Stresses in hollow nanoparticles. Int. J. Solids Struct. 2010; 47, 2799–2805. (DOI:10.1016/j.ijsolstr.2010.06.008)